Table 1 Experimental conditions

Flow rate, kg/sec					
Total	1.26	1.51	2.0	2.52	3.0
Diesel oil (C/H/S = 85.4/14.2/0.3)	0.2	0.257	0.37	0.482	0.592
Oxygen	0.682	0.87	1.245	1.62	1.985
KOH solution	0.036	0.044	0.059	0.074	0.089
Atomizing N_2	0.341	0.341	0.341	0.341	0.341
Thermal input, MW	8.4	10.8	15.6	20.3	24.9
Combustor pressure, atm	1.46	1.72	2.28	2.84	3.52
Running time, minutes	15	35	30	26	59

calculated pressure distribution shows considerable disagreement in the neighboring region. The position of the shock wave moves upstream as the load increases.

Figure 3 shows the open voltage and short-circuit current distribution for the mass flow rate of 3.0 kg/sec. The small numbers (1-50) in the figure indicate electrode numbers and their positions. The analysis gives extremely good agreement on open voltage. The small deviation is due to the leakage current, judging from the measurement by probes of the potential distribution in the Faraday direction. The decline of the voltage at the end of generating section is due to the steep drop of the magnetic field. The measured electrode drop by probe was about 400 V at the No. 14 electrode and about 500 V at the No. 26 electrode. The relatively large current could be extracted in spite of the large voltage drop of the cold boundary layer. The calculated short-circuit current shows some deviation from the measured value, especially in the downstream region.

The maximum output power of 482 kW and the total short-circuit current of 2820 A were obtained for the mass flow rate of 3 kg/sec. The Hall voltage (and Hall field intensity) for the mass flow rate of 3 kg/sec were 2525 V (19.61 V/cm), 2075 V (11.11 V/cm), 1685 V (7.84 V/cm), and 1160 V (5.88 V/cm) as load increased. The calculated maximum output power, total short-circuit current, and Hall voltage at short circuit were 429 kW, 2600 A, and 4000 V, respectively.

Concerning the superconducting magnet, a very long time is needed to cool and magnetize the magnet which was composed of the Nb-Ti-Zr coil of 13 tons and the support of 35 tons. The required time to cool the magnet from 300 K to 150 K by cold He gas was 124 hr, from 150 K to 50 K, by refrigerating operations was 97 hr, and from 50 K to 15 K was 25 hr. The time to liquify the He gas and charge the liquid He in a cryostat was 76 hr. The raising time (5-15 A/min) of the magnetic field until 4.2 T was 13 hr.

We may conclude that this generator can extract high output power and endure for a long time judging from the good durability at least for 12 hr, (4 hr × 3 times) under the thermal flux of 270 W/cm^2 at the nozzle throat for the mass flow rate of 2.5 kg/sec without any replenishment, and also based on the ETL Mark III's result of 230 hr endurance.

The quasi-one-dimensional analysis could predict the generating characteristics within an error of 15%. However, further work is needed to improve the understanding of the heat loss, the leakage current, and the electrode phenomena in regard to the seed compound.

References

[1]Fushimi, K., et al., "Construction of an MHD Generator with A Large-Scale Superconducting Magnet (ETL Mark V)", *Proceedings of the 13th Symposium on Engineering Aspects of MHD,* 1973, Stanford University, Stanford, Calif.

[2]Fushimi, K., et al., "Experiment on MHD Generator with a Large-Scale Superconducting Magnet", *Proceedings of the 14th Symposium on Engineering Aspects of MHD,* 1974, University of Tennessee Space Institute, Tullahoma, Tenn.

[3]Aiyama, Y., "Research on Superconducting Magnet System for MHD Project in Japan", *Proceedings of the 5th International Cryogenic Engineering Conference,* 1974, Kyoto, Japan.

[4]Aiyama, et al., "A Large Superconducting MHD Magnet", *Proceedings of the 5th International Cryogenic Engineering Conference,* 1974, Kyoto, Japan.

[5]Aiyama, Y., et al., "Helium Refrigerator-Liquifier System for MHD Generator", *Proceedings of the 5th International Cryogenic Engineering Conference,* 1974, Kyoto, Japan.

[6]Ikeda, S., et al., "Experiment on MHD Generator with a Large-Scale Superconducting Magnet", *Proceedings of the 15th Symposium on Engineering Aspects of MHD,* 1976, University of Pennsylvania, Philadelphia, Pa.

Skin Friction on a Flat Perforated Acoustic Liner

Donald R. Boldman* and Paul F. Brinich†
NASA Lewis Research Center, Cleveland, Ohio

Nomenclature

a = local speed of sound
b = cavity depth
C_f = skin friction coefficient
d = diameter of holes in perforated plate
f = frequency
L = reference length along acoustic liner
l = effective thickness of perforated plate (includes orifice end correction)
Re = Reynolds number
S = Strouhal number
U_∞ = freestream velocity
x = axial distance along wind tunnel wall
y = distance from wall
δ^* = boundary-layer displacement thickness
θ = boundary-layer momentum thickness
σ = ratio of hole area to total area on perforated plate
χ = linear reactance
$()_0$ = denotes condition at upstream station referenced to the virtual origin of the boundary layer

Introduction

IT has been well-established that acoustic treatment of the ducts in turbomachinery provides an effective means for reducing external noise levels. One type of acoustic material consists of an array of honeycomb cavities covered with a perforated plate with flow passing along it. However, the roughness associated with a perforated surface can increase the skin friction coefficient. Although much is known about roughness effects on friction for surfaces containing certain types of roughness elements such as sand grains, ribs, threads,

Received Aug. 4, 1976.
Index categories: Boundary Layers and Convective Heat Transfer – Turbulent; Aircraft Noise, Powerplant.

*Aerospace engineer, Fluid Physics and Chemistry Branch of the Physical Sciences Division. Member AIAA.

spheres, etc., little is known about friction coefficients associated with perforated acoustic liners. In the latter case, the holes in the surface plate provide active sites of turbulence production. This report concerns the measurement of friction coefficients of a typical perforated acoustic liner installed in the side of a wind tunnel. The results are compared with measured friction coefficients of a smooth hard wall for the same mean flow velocities in a wind tunnel.

In addition to the surface roughness effects on skin friction, it is also conceivable that under certain conditions an alternating inflow and outflow of fluid stimulated by the passage of sound waves could affect the skin friction. This pumping of fluid at the perforated surface of acoustic liners has been confirmed in studies reported in Refs. 1 and 2 and elsewhere. A detailed investigation of the influence of this pumping action on the friction coefficient could not be conducted in the wind tunnel because of a high background flow noise. However, certain observations concerning this aspect are discussed for the special case of a very low velocity operating condition ($U_\infty = 18$ m/sec) in which imposed random noise altered the mean boundary-layer profiles. At this low velocity condition the imposed noise was greater than the flow noise.

Experiment

Local skin friction coefficients on a smooth flat hard wall (reference case) and on a flat perforated acoustic liner were determined from boundary-layer momentum surveys performed in a 10 by 25 cm wind tunnel shown schematically in Fig. 1. A 25 by 122 cm smooth or acoustic panel, installed in the side wall of the wind tunnel, provided the test surface for the boundary-layer measurements. As shown in Fig. 1 the acoustic panel consisted of a 0.051 cm-thick perforated plate backed by a structure of hexogonal cells 0.95 cm in diameter by 0.64 cm deep, and mounted on a solid plate. The open area ratio of the staggered hole perforated plate was 0.08 with a hole diameter of 0.127 cm.

Boundary-layer surveys, obtained with a 0.07 cm-diameter round pitot probe at different axial stations, provided the axial distribution of momentum thickness θ and displacement thickness δ^* required for estimation of the local skin friction coefficient C_f. At the velocities of primary interest (61, 122, and 213 m/sec), 10 boundary-layer surveys were made on the acoustic wall and four on the smooth wall. These surveys were made by continuously traversing the pressure probe across the boundary layer at a given axial station. At a low velocity condition of 18 m/sec, where noise sources were employed, two surveys were made on the acoustic wall. In this case the measurements were obtained using 90 sec integrated average values at each point in the boundary layer. This rather time-consuming process was necessary because of large-amplitude, low-frequency oscillations in the boundary layer.

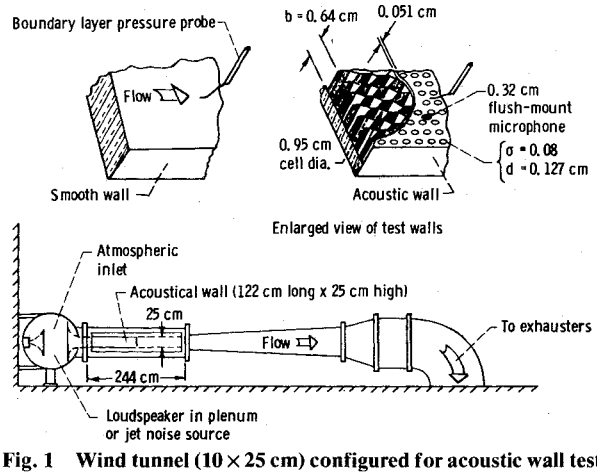

Fig. 1 Wind tunnel (10 × 25 cm) configured for acoustic wall tests.

A flush-mounted microphone was located near the centerline of the acoustic wall approximately 46 cm downstream of the leading edge of the panel. This microphone was used to determine the sound spectra near the acoustic wall and thus provide information for tuning the liner section. A 60 W loudspeaker and jet noise source were installed in the plenum.

The loudspeaker could produce either a single frequency tone or a broadband random noise, both of about 110 dB intensity measured in the test section, and the air jet produced a broadband noise of about 110 dB.

Experimental Friction Results

Several methods for experimentally determining the skin friction on a flat wall have been described in the literature. In general these methods include direct measurement techniques, which commonly use a floating element at the surface of the wall, as well as indirect methods, which involve boundary-layer, mean-velocity measurements. In both methods extreme care must be exercised in making the measurements. For instance, in the direct methods factors such as the pressure gradient on either side of the floating element can introduce large corrections to the measurements, whereas in the indirect boundary-layer approach the friction coefficient must be obtained by differentiating experimental boundary-layer momentum thickness distributions along the wall. The latter method, with its inherent problems, was chosen for the present study because of potentially greater problems in designing a floating element gauge compatible with thick acoustic walls.

In reducing the data, smoothed experimental distributions of $\theta(x), \delta^*(x)$, and $U_\infty(x)$ were incorporated in the integral form of the momentum equation[3] given by

$$\theta - \theta_0 + \int_{x_0}^{x} \left\{ \left[2 + \frac{\delta^*}{\theta} - \left(\frac{U_\infty}{a} \right)^2 \right] \frac{\theta}{U_\infty} \frac{dU_\infty}{dx} \right\} dx = \int_{x_0}^{x} \frac{C_f}{2} dx \tag{1}$$

Smoothing of the boundary-layer data was achieved by means of a least squares fit though the logarithmic distributions of $\theta(x)$ and $\delta^*(x)$. The distance from the virtual origin to the upstream station on the test wall x_0 was calculated from the

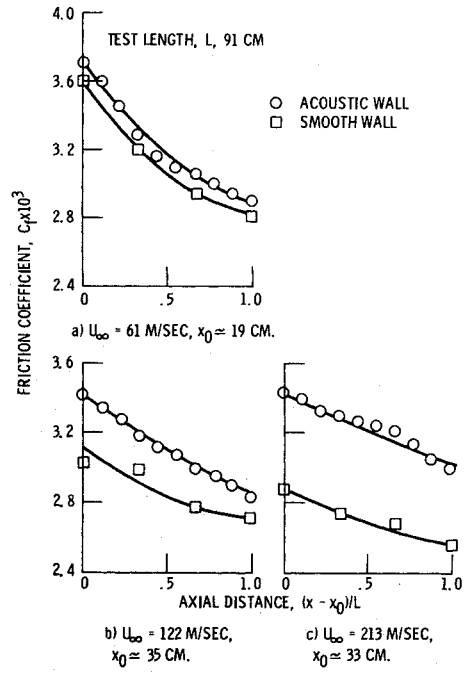

Fig. 2 Experimental friction coefficients based on boundary-layer momentum surveys at high freestream velocities ($61 \leq U_\infty \leq 213$ m/sec).

flat plate relationship for a turbulent boundary layer[3] commonly expressed as

$$\theta_0 = 0.036 x_0 Re_{x_0}^{-0.2} \tag{2}$$

where θ_o represents the measured value of momentum thickness at the upstream station.

Differentiation of Eq. (1) yields the following expression for the local skin friction coefficient

$$\frac{d}{dx}\int_{x_0}^{x} C_f dx = C_f(x) \tag{3}$$

In Fig. 2 the local friction coefficients for the acoustic wall, obtained by numerical differentiation of the left side of Eq. (1), are compared with the values for the hard wall. At a velocity of 61 m/sec, an increase in C_f of only a few percent can be observed whereas at the highest velocity of 213 m/sec an increase in friction of about 20% was obtained. This behavior is characteristic of a rough wall in which an effective sand grain roughness height can be assigned to a given acoustic surface. In classical roughness theories, the most significant effect of roughness on the friction coefficient would occur at the highest velocity where the ratio of boundary-layer thickness to effective roughness height attains its lowest value.

From the standpoint of surface roughness effects, the friction could possibly be reduced by decreasing the hole size since the holes provide active sites of turbulence production. However, such alternatives would have to be compatible with the desired sound attenuation characteristics of the liner. Some observations of these sound attenuation characteristics are given in the following section.

Flow with Imposed Noise

A few tests were performed to determine whether changes in the boundary layer could be observed when noise was introduced from the various noise generators in the plenum. Broadband noise sources consisting of an air jet and a random noise generator were used to determine the frequency for optimum sound attenuation. These noise sources had a nearly flat output up to 10 and 6 kHz (speaker cutoff), respectively. Sound pressure level spectra from the flush mounted microphone indicated that the frequency for optimum sound attenuation by the liner was about 4.8 kHz. This is indicated by the frequency of the minimum in the sound pressure level spectrum shown in Figs. 3a and b for the jet and random noise generator sources. Although these spectra were obtained with no flow, the frequency of minimum sound pressure level did not change noticeably with freestream velocities up to about 20 m/sec.

When the freestream velocity reached about 30 m/sec the imposed noise disappeared into the higher background noise produced by the turbulence in the flow as shown in Fig. 3c for the jet noise source. Actually an increase in sound pressure level can be observed at the liner resonant frequency of 4.8 kHz.

This spike in the sound pressure level spectrum is believed to represent self-generated noise of the type described in Ref. 4. Self-generated noise in a hydrodynamic flowfield ($d \ll a/f$) occurred at a Strouhal number ($S = fd/U_\infty$) of about 0.2 (Ref. 4). Accordingly, at a freestream velocity of 30 m/sec and a hole diameter of 0.127 cm, the frequency for self-generated noise would be about 4.7 kHz.

The observed value of resonant frequency for the liner was calculated from the expression for the reactance of Helmholtz resonator arrays[5] by setting the reactance equal to zero. In this case

$$\chi = 0 = (2\pi \ell f/\sigma a) - \cot(2\pi f b/a) \tag{4}$$

where the expression for ℓ, the effective perforated plate thickness, is given in Ref. 6. The calculated resonant frequency for the liner was 4.8 kHz, which is consistent with the minimum in the attenuation spectra. It is recognized that the resonant frequency is not necessarily the frequency for optimum damping since the optimum frequency depends on the particular modes of propagation.[7] However, in the present experiment, the optimum tuned frequency based on the broadband noise spectra appears to be equal to the calculated resonant value for the liner.

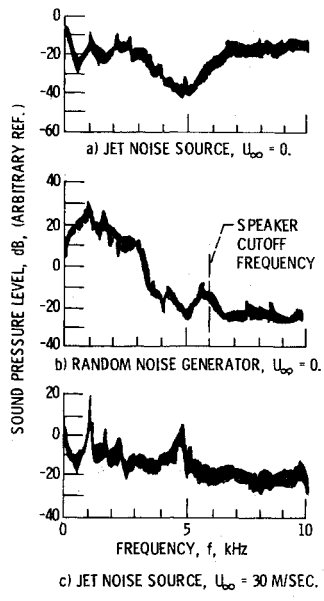

Fig. 3 Narrow band sound spectra for acoustic wall.

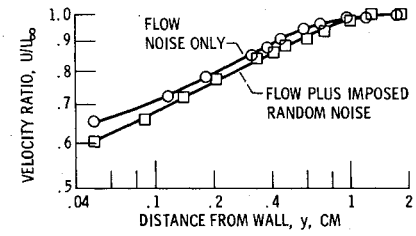

Fig. 4 Effect of imposed random noise on the acoustic wall boundary layer at a low velocity. $U_\infty = 18$ m/sec; $x/L = 0.67$.

Boundary-layer mean velocity profiles are presented in Fig. 4 for flow over the acoustic liner with and without random noise introduced from the plenum. These velocity profiles, obtained at $x/L = 0.67$, show differences which result in an increase in the boundary-layer momentum thickness with imposed noise. This thicker boundary layer (larger value of θ) suggests a higher friction coefficient with imposed noise. The boundary layer on the hard wall remained essentially the same when noise was introduced.

Since the frequency for optimum sound attenuation was found to be about 4.8 kHz, it was of interest to introduce a tone at this frequency to determine whether a similar change in the boundary layer could be observed. Surprisingly, however, the introduction of a 4.8 kHz tone at the same overall sound pressure level did not alter the boundary layer (implying no change in skin friction). This result is attributed to differences in the mode of propagation of the various imposed noises. Since the optimum frequency depends on the particular sound propagation modes,[7] it is conceivable that the optimum frequency for the tone was not the same as the frequency corresponding to the minimum sound pressure level for the broadband noise sources shown in Fig. 3.

Conclusions

Although the results of this study of friction cannot currently be extrapolated to include other liner geometries, it is

significant to note that the 20% increase in friction at a velocity of 213 m/sec (a realistic velocity for turbo-machinery components utilizing such liners) represents a loss in performance. Furthermore, under certain conditions there appears to be an increase in friction due to imposed noise. This conclusion is based on changes in the mean boundary layer with imposed noise; however this effect was noted only at low velocity levels ($U_\infty = 18$ m/sec).

References

[1]Baumeister, K. J. and Rice, E. J., "Visual Study of Effect of Grazing Flow on the Oscillatory Flow in a Resonator Orifice," TM X-3288, 1975, NASA.

[2]Rogers, T. and Hersh, A. S., "The Effect of Grazing Flow on the Steady State Resistance of Square-Edged Orifices," AIAA Paper 75-493, Hampton, Va., 1975.

[3]Schlichting, H., *Boundary Layer Theory,* McGraw-Hill, 1960.

[4]Bauer, A. B. and Chapkis, R. L., "Noise Generated by Boundary Layer Interaction with Perforated Acoustic Liners," AIAA Paper 76-41, Washington, D.C., 1976.

[5]Groeneweg, J. F., "Current Understanding of Helmholtz Resonator Arrays as Duct Boundary Conditions," *Basic Aerodynamic Noise Research,* R. Schwartz, Ed., SP-207, 1969, NASA, pp. 357-368.

[6]Rice, E. J., Feiler, C. E., and Acker, L. W. "Acoustic and Aerodynamic Performance of a 6-Foot-Diameter Fan for Turbofan Engines. Part III-Performance with Noise Suppressors," TN D-6178, 1971, NASA.

[7]Rice, E. J., "Spinning Mode Sound Propagation in Ducts with Acoustic Treatment," TN D-7913, 1975, NASA.

Similarity Solution of the Boundary-Layer Equations for Laser Heated Flows

Peter K. Wu*
Physical Sciences Inc., Woburn, Mass.

Introduction

RECENT developments in high-power CO_2 lasers have made it feasible to consider adding large amounts of energy to a gas flow via the absorption of 10.6μ laser radiation by inverse Bremsstrahlung and the conversion of the absorbed energy into KE. This concept can be applied to laser propulsion[1-3] and the hypersonic wind tunnel.[4] More recently the one-dimensional steady nozzle flow with laser energy addition has been examined.[5-6] When the flow medium in a laser-heated rocket thruster is pure hydrogen, which has been chosen on specific impulse considerations, the average temperature of the hot plasma core is about 14,000 K[6], and the core Reynolds number based on the nozzle throat diameter is approximately 2000. In the absence of mass injection to protect the wall, the convective heating will be severe under such high freestream temperature. To estimate the heat-transfer rate to the wall, we solve the laminar boundary-layer equations with local similarity approximation.

Received July 9, 1976; revision received Aug. 11, 1976. This work was sponsored by NASA Lewis, under Contract NAS3-19695 and NASA Project Manager, Stephen M. Cohen. The author expresses his appreciation to N. Kemp for reviewing the manuscript and his helpful comments.

Index categories: Boundary Layers and Convective Heat Transfer—Laminar; Lasers; Radiatively Coupled Flows and Heat Transfer.

*Principal Scientist. Member AIAA.

Laminar boundary layers exhibiting similarity have long played an important role in exposing the principal physical features of boundary-layer phenomena and in providing a basis for approximate methods of calculating more complex, nonsimilar cases. Here, the transport properties vary significantly across the boundary layer under such extreme temperature variation (the $\rho\mu$, density-viscosity, product at the wall can be 10 times the freestream value). The existing similarity solutions with variable transport properties, i.e., Ref. 7, only cover the ratio of $\rho\mu$ product up to a factor of about 3. In addition hydrogen at 3 atm is completely dissociated at about 5000 K. Hence the boundary-layer equations with variable transport properties have been solved by a quasilinearization technique[8] and the equilibrium properties of hydrogen[9-10] have been used in the calculations.

Method of Analysis

For simplicity, we assume that Prandtl number $Pr=1$ and $\rho \sim h^{-1}$ where h is the enthalpy. A simple extension of the Cohen-Reshotko[11] analysis by including variable $\rho\mu$ will provide the following similar boundary-layer equations

$$[(\rho\mu/\rho_e\mu_e)f_{\eta\eta}]_\eta + ff_{\eta\eta} + \beta(g - f_\eta^2) = 0 \quad (1)$$

$$[(\rho\mu/\rho_e\mu_e)g_\eta]_\eta + fg_\eta = 0 \quad (2)$$

with boundary conditions $f(0)=f_\eta(0)=0$, $g(0)=g_w$, $f_\eta(\infty)=g(\infty)=1$ where $f_\eta = u/u_e$ is the nondimensional velocity; $g=h_s/h_{se}=(h+u^2/2)/h_{se}$ is the stagnation enthalpy ratio; and the subscripts e and s indicate the external and stagnation conditions, respectively. The similarity variables are

$$\xi = \int_0^x r^{2j}\rho_e\mu_e u_e \mathrm{d}x$$

$$\eta = (\rho_e u_e/\sqrt{2\xi})\int_0^y r^j \frac{\rho}{\rho_e}\mathrm{d}y$$

and the pressure gradient parameter is

$$\beta = \frac{2\xi}{u_e}\frac{\partial u_e}{\partial \xi}\left(\frac{h_{se}}{h_e}\right)$$

The superscripts $j=0$ and 1 correspond to the two-dimensional and the axisymmetric cases, respectively. Equations (1) and (2) can now be solved by quasilinearization

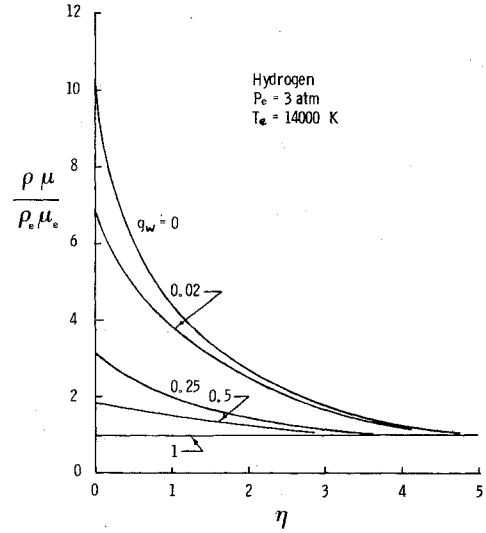

Fig. 1 Variation of density-viscosity product across the boundary layer.